minerals

MDPI

Article

Characterization of Incremental Markings in the Sagittal Otolith of the Pacific Sardine (*Sardinops sagax*) Using Different Imaging Modalities

Kelsey C. James [1], Uwe Kierdorf [2], Victoria Cooley [3], Viktor Nikitin [3], Stuart R. Stock [4,*] and Horst Kierdorf [2]

[1] Southwest Fisheries Science Center, National Marine Fisheries Service, NOAA, La Jolla, CA 92037, USA; kelsey.james@noaa.gov
[2] Department of Biology, University of Hildesheim, 31141 Hildesheim, Germany; kierdo@uni-hildesheim.de (U.K.); kierdorf@uni-hildesheim.de (H.K.)
[3] The Advanced Photon Source, Argonne National Laboratory, Lemont, IL 60439, USA; vcooley@anl.gov (V.C.); vnikitin@anl.gov (V.N.)
[4] Department of Cell and Developmental Biology, Feinberg School of Medicine, and Simpson Querrey Institute, Northwestern University, Chicago, IL 60611, USA
* Correspondence: stuart.r.stock@gmail.com

Abstract: Teleost fish possess calcium carbonate otoliths located in separate chambers (utriculus, sacculus, and lagena) of their membranous labyrinth. This study analyzed the surface topography of the sagittal otolith of the Pacific sardine (*Sardinops sagax*) and the daily and annual increments in these otoliths. The otolith surface, characterized by laser scanning confocal microscopy for the first time, consisted of a system of prominent ridges and valleys (grooves), but it is unclear whether these structures are functional or represent time-resolving markings reflecting growth periodicity. Within the first-year volume, daily increments, each consisting of an incremental (more mineralized) and a discontinuous (less mineralized) zone, were resolved by optical microscopy and backscattered electron (BSE) imaging in the scanning electron microscope (SEM). Daily growth increments could, however, not be resolved in volumes formed after the first year, presumably because otolith growth markedly slows down and spacing of incremental markings narrows in older fish. Throughout otolith growth, the crystalline network continues across the discontinuous zones. Fluorochrome labeling provides additional information on growth after the first year. Compared with optical and BSE imaging, synchrotron microComputed Tomography of intact otoliths (with 0.69 µm volume elements) was less able to resolve daily increments; X-ray phase contrast reconstructions provided more detail than reconstructions with absorption contrast. Future research directions are proposed.

Keywords: fluorochrome labeling; laser scanning confocal microscopy; recording structure; scanning electron microscopy; sclerochronology; synchrotron microCT imaging

check for updates

Citation: James, K.C.; Kierdorf, U.; Cooley, V.; Nikitin, V.; Stock, S.R.; Kierdorf, H. Characterization of Incremental Markings in the Sagittal Otolith of the Pacific Sardine (*Sardinops sagax*) Using Different Imaging Modalities. *Minerals* **2024**, *14*, 705. https://doi.org/10.3390/min14070705

Academic Editors: Emeline Raguin, Steve Weiner and Alejandro B. Rodriguez-Navarro

Received: 3 May 2024
Revised: 25 June 2024
Accepted: 8 July 2024
Published: 12 July 2024

1. Introduction

Several animal mineralized tissues are recording structures, sensu Klevezal [1], documenting either part of or the entirety of an animal's life. Mammalian dental enamel is an example of the former [2]. Examples of the latter include mammalian tooth cementum [3], mollusk shells [4,5], and shark vertebral centra [6], although, in the last example, the ability to resolve growth zones is limited in older individuals due to the small amount of material deposited in each zone.

The field of study addressing the reconstruction of life history traits of recent or fossil organisms and their environments based on the analysis of these recording structures is known as sclerochronology [7]. The discipline has been defined as "the study of physical and chemical variations in the accretionary hard tissues of organisms, and the temporal context in which they are formed" (Oschmann [8], p. 1). Fish otoliths are another such recording structure, and growth zones in otoliths are widely used for age estimation in fish [9–11].

The inner ear of teleost fishes contains solid otoliths (“ear stones”) that are located in separate chambers (utriculus, sacculus, and lagena) of the membranous labyrinth and function in the perception of linear accelerations (including gravitational forces) and hearing [12]. The three otoliths per labyrinth vary in size and shape and are referred to as lapillus (from utriculus), sagitta (from sacculus), and asteriscus (from lagena), with the sagittal otolith in most species being the largest of the three [13,14]. The huge range in the size and shape of teleost otoliths has been linked to whole-genome duplication events and the subsequent sub- or neo-functionalization of the duplicated genes [12].

Otoliths are acellular biomineralized structures composed of a mineral phase and an organic matrix, the latter accounting for $\leq$10% of the otolith mass [9,15]. The mineral phase is calcium carbonate ($CaCO_3$), mostly in the form of aragonite, while the organic matrix consists of proteins and proteoglycans [9,12,16,17]. The seeding and growth of otoliths are under the control of regulatory proteins from the surrounding endolymphatic fluid [17].

In the otolith end organs, the sensory epithelium, referred to as the macula, is overlain by the otolith. The contact between macula and otolith is mediated by an acellular matrix, the otolithic membrane [12,18], with the three structures forming a functional unit. The otolithic membrane is composed of a fibrous layer, which directly overlies the ciliary bundles of the sensory hair cells and also covers portions of the adjacent non-sensory epithelium, and a gelatinous layer [12]. Each ciliary bundle consists of a kinocilium and a group of stereovilli, and stimulation of the macular hair cells is brought about by deflection of the ciliary bundles [12,19].

Otoliths of teleost fishes grow throughout life, with daily accretion of new growth layers [20–23]. In addition to daily increments, which reflect a circadian growth rhythm, otoliths also exhibit incremental structures reflecting infradian (supradaily) growth cycles, such as (semi-) lunar and annual increments [20,22,24]. Furthermore, subdaily increments have been described, which can be mistaken for daily growth increments [22].

The continual accretion of material to the otolith over time serves to maintain the size and shape of the otolith, enabling the fish to receive certain sound frequencies and maintain body orientation [12,25,26]. Each additional layer is deposited on a diel cycle and mediated by calcium and protein concentrations in the endolymph [26–28]. The periodically formed growth layers serve as a permanent record from which age, ambient environmental conditions, and other information can be determined [10,12,29]. An otolith increasing in size at a predictable, age-dependent rate is key for its use to determine age [22,30].

Daily and annual increments of otoliths have been extensively used to track larval [31] and adult fish growth [32]. The periodicity of these structures has been investigated with good support for daily and annual growth cycles across numerous species [22,33,34]. However, many studies still assume daily or annual periodicity without conducting age validation studies, which are labor-intensive and time-consuming [35]. The increasing sophistication of techniques such as backscattered electron (BSE) imaging of polished sections or microComputed Tomography (microCT) of entire otoliths may offer promise for validation studies.

The Pacific sardine (*Sardinops sagax*) is an economically important forage fish in the Northeastern Pacific Ocean that is short-lived and fast-growing [36]. Most of the somatic and otolith growth of Pacific sardines occurs in the first two years of life [36], and therefore they make a good candidate to examine otolith growth and microstructure. The species would benefit from additional age validation because annual ages are incorporated into the Pacific sardine stock assessment [37], and, as of yet, not all age classes have been validated [11,38,39].

The study reported below applies BSE imaging, optical microscopy, including laser scanning confocal microscope (LSCM) imaging, and synchrotron microCT imaging to characterize the incremental markings in otoliths of the Pacific sardine. The specific focus is the appearance of the markings depending on the imaging modalities used for their visualization.

2. Materials and Methods

The terminology referring to incremental markings in fish otoliths is varied, and a clear definition of terms is required to avoid ambiguity. ‘Increment’ has been defined by Buckmeier et al. [30] (p. 35) as “a general term describing the growth of a calcified structure during a specific time interval (e.g., annual or daily)”. We qualify the term increment with the appropriate descriptor (e.g., annual increment). A zone is defined as “a region of similar structure or of similar optical appearance within a calcified structure” [30] (p. 36). We use ‘incremental marking’ to denote a structural feature (of an otolith) that allows the identification of increments and thereby the reconstruction of growth cycles. An overview of some common terms used to describe daily incremental markings of otoliths, as well as the appearance of these markings depending on the methods used for their visualization, is given in Table 1.

Table 1. Synopsis of the terminology and appearance of daily incremental markings in fish otoliths. A daily growth increment is a bipartite structure consisting of an incremental zone and a discontinuous zone according to the terminology introduced by Mugiya et al. [21].

Authors/Methods	Incremental Zones	Discontinuous Zones
Mugiya et al. [21]	calcium-dominant zones	matrix-dominant zones
Dunkelberger et al. [18]	calcified layers	layers of organic matrix/interlamellar matrix
Hay et al. [40] (XRF spectromicroscopy)	light (L) zones (low sulfur content)	dark (D) zones (high sulfur content)
Campana and Neilson [22] (SEM-SE images of etched surfaces)	lightly etched zones	deeply etched zones
Reflected light images of polished block surfaces	broader, translucent zones	narrower, opaque zones
SEM-BSE images of polished block surfaces	broader, bright zones	narrower, dark zones
Transmitted light and reflected plain light (bright background) images of thin ground sections	broader, bright zones	narrower, dark zones
Polarized transmitted light images of thin ground sections	broader, bright zones	narrower, dark zones

2.1. Samples

Pacific sardine sagittal otoliths (sagittae) were collected during fishery-independent surveys conducted by Southwest Fisheries Science Center, La Jolla, CA, USA (Table 2). One captive individual (#83, age 0 years) was injected with oxytetracyline (OTC, Liquamycin La-200® (the use of Trade Names does not imply endorsement from the National Oceanic and Atmospheric Administration), 200 mg mL^{-1}) at a dosage of 100 mg/kg body weight and sacrificed one year after the injection; this sample was from an earlier study [11]. Both sagittal otoliths were extracted, rinsed with water, air-dried, and stored in labeled plastic microtubes until analysis. All imaging and measurements were performed on otoliths from the right side.

Table 2. Biological data of Pacific sardine samples analyzed in this study. The standard length of the fish is the length from the tip of the snout to the posterior end of the hypural plate. The age is the number of completed years based on a 1 July birthdate. The otolith radius is the distance between the center of the otolith's focus and the most posterior point of the otolith.

Sample Number	Date Collected	Standard Length (mm)	Age	Otolith Radius (mm)
4	21 August 2016	190	1	1.35
7	21 July 2017	223	6	1.59
13	2 August 2017	196	2	1.36
14	9 August 2017	103	0	0.86
83	3 February 2016	185	1	1.43

2.2. Whole Otolith Ageing

The sagittal otoliths were aged following Yaremko [41]. In brief, the otoliths were submerged in water and viewed on a black background at 25× magnification with reflected light using a stereomicroscope (MZ10 F, Leica Microsystems, Vienna, Austria). Annual increments composed of one opaque zone and one translucent zone were counted from the focus to the posterior edge. An annual increment is complete at the interface of an inner translucent zone and a distal opaque zone [41,42]. Age was assigned to each fish based on the number of annual increments, the date of capture, a 1 July birthdate (following Yaremko [41], the birthdate is a date agreed upon for U.S. fishery management after which all fish are considered a year older and does not refer to the actual hatching date of each Pacific sardine), and the distal zone present on the margin. Ages are reported to the year; partial annual increments on the otolith margin or date of capture were not used to calculate a fractional age.

2.3. Otolith Surface Imaging

The unembedded otoliths were first viewed and photographed in air under reflected light using a digital microscope (Keyence VHX 7000, Keyence, Osaka, Japan) equipped with a wide-range (100× to 1000× magnification) zoom lens (Keyence VH-Z 100T). Additional images were acquired with a Keyence VK-X1000 LSCM equipped with a 661 nm laser, using either a ×5 objective (working distance 22.5 mm) or a ×20 objective (working distance 11 mm).

Prior to surface-imaging in the scanning electron microscope (SEM), the otoliths were sputter-coated with a thin layer (thickness 12 nm) of gold-palladium in a Leica EM ACE200 low-vacuum coater (Leica Microsystems, Vienna, Austria). The coated specimens were then viewed in a Zeiss Evo Ma 15 SEM (Carl Zeiss, Oberkochen, Germany) operated in the secondary electron (SE) mode at 10 kV.

2.4. Embedding, Sectioning and Polishing of Otoliths

Following the acquisition of surface images, the otoliths were embedded in epoxy resin (Biodur E12/E1, Biodur products, Heidelberg, Germany). The embedded specimens were manually ground and dry-polished along their anterior–posterior axis until the desired section depth (plane running through the focus) was almost reached, using a graded series of silicon carbide sandpapers. This was followed by a final wet-polishing on a motorized rotary polisher (Labopol-5, Struers, Ballerup, Denmark), first using a diamond suspension of 3 µm particle size (DiaPro, Struers) and then a water-based slurry made from 0.3 µm aluminum powder (AP-D powder, Struers).

For the production of thin ground sections, the embedded and ground otoliths were mounted with their polished surface down on glass slides. The mounted blocks were then ground and dry-polished from the other side to a final thickness of approximately 60 µm, employing graded silicon carbide sandpaper and a final polishing step using a leather cloth and a solid polishing compound (Menzerna, Ötigheim, Germany).

2.5. Imaging of Polished Sectional Block Surfaces of Otoliths

The polished block surfaces of the otoliths were first viewed and photographed under reflected light in the Keyence VHX 7000 digital microscope. Subsequently, BSE imaging of the (uncoated) polished surfaces, which were oriented perpendicular to the primary electron beam, was performed in the Zeiss Evo Ma 15 SEM at a 20 kV accelerating voltage, using a high-resolution BSE detector. The gray-level variation in BSE images of topographically flat mineralized tissues reflects local variation in the degree of mineralization, with brighter or darker gray levels characterizing areas of higher or lower mineral content, respectively [43,44].

2.6. Light Microscopic (LM) Imaging of Otolith Ground Sections

Micrographs of the thin ground sections were obtained in the Keyence VHX 7000 digital microscope as well as Zeiss Axioskop 2 plus and Zeiss Axio Imager 2 microscopes equipped with digital cameras (Zeiss Axiocam 503 color and Axiocam 506 mono), using plain transmitted or reflected light, linearly polarized transmitted light (sometimes with a 1λ plate), and epifluorescence imaging. Images of the ground sectioned from the OTC-labeled otolith were obtained with the monochromatic Zeiss Axiocam 506 camera and a ×40 objective. The same area was first photographed using brightfield illumination, followed by imaging using a GFP filter set (excitation wavelength 493 nm, emission wavelength 513 nm). The collected fluorescence light was converted from grayscale to green using the processing software (Zeiss ZEN 2.6) of the microscope. An overlay image of the two recording channels (brightfield and fluorescence) was then produced using the same software.

2.7. Image Processing, Counting, and Comparison of Incremental Features

The acquired images were processed and arranged into plates using Adobe Photoshop CS4 software (Adobe products, San Jose, CA, USA). As the whole otolith images and the images of the polished block surfaces have a reversed anterior–posterior orientation compared to those of the ground sections, some images were flipped horizontally to achieve a consistent orientation within a single plate. Incremental markings were identified in both the SEM and LM images, and the appearance of these markings in micrographs obtained with different imaging modalities was compared.

2.8. Synchrotron microComputed Tomography (MicroCT)

Synchrotron microCT was performed at beamline 2-BM, the Advanced Photon Source (APS), Argonne National Laboratory, Lemont, IL, USA, with 24 keV X-rays; see [45] for a beamline description. Each whole otolith (Table 2) was imaged separately in its microtube. A total of 3000 projections (0.3 s exposure/projection) were collected over 180° specimen rotation, and there was a 100 mm separation between the sample and detector scintillator. Reconstructions were performed with 0.69 µm isotropic volume elements (voxels), whereby each slice consisted of 2448 × 2448 voxels and there were 2049 slices per field of view (FOV). The reconstructed data (32-bit float) totaled 45.7 GB/FOV. The volume of otolith #7 was also reconstructed with X-ray phase contrast using the Paganin algorithm [46] as implemented in TomocuPy [47].

The alignment of the otolith anatomical axes was highly variable relative to the microCT slice plane. The absorption contrast microCT data were imported into Fiji [48] in stacks of 500 slices and resliced to the coronal plane. Brightness and contrast were adjusted to enhance the incremental markings. Stacks were scrolled through manually to identify the slice(s) that ran through the focus. A slice was chosen based on its proximity to the focus and the clarity of incremental markings. The same slice was chosen among resliced stacks to create a composite image from the focus to the posterior margin in the coronal plane. Low-density zones (zones with dark contrast) were identified, marked, and counted from the focus to the posterior margin in Adobe Photoshop. This was not possible for the entire radius of each otolith. The width of each high- or low-density zone was measured wherever low-density zones had been counted.

A 3D rendering of otolith #7 from the absorption contrast microCT data was produced using Dragonfly software (version 2021.3.0, Object Research Systems, Montreal, QC, Canada). Contrast from the wall of the container (containing the otolith) was cropped, and the window level and gamma were adjusted to render the air transparent. A flat plane was used to generate a digital cut-away view of the 3D rendering.

3. Results

We first describe the overall surface structure of the otoliths and also shortly address the issue of age-dependent variation in the otolith growth rate. Next follows a description of daily increments and a comparison of different imaging modalities regarding their ability to resolve these increments. The appearance of annual increments is then compared between surface images and ground sections. Finally, the potential of microCT to provide details of the otolith surface and internal structure is explored, and the result of fluorochrome labeling of an otolith is reported.

3.1. Otolith Surface Structure and Variation of Growth Rate

Figure 1 shows the general external morphology of Pacific sardine sagittal otoliths and demonstrates their high structural complexity. The otoliths are longer along the anterior–posterior than the dorso–ventral axis, indicating that markedly more material is being added per unit of time along the former than the latter. The rostrum is much larger than the antirostrum, and there is a prominent excisura major at the anterior end, while the excisura minor at the posterior end is only weakly developed. The otolith's ventral edge is often serrated (Figure 1a,b and Figure 2c), while its dorsal edge shows a more undulating shape (Figure 1a,b). The otolith's lateral surface is convex and exhibits numerous prominent ridges running parallel to the outer margin of the otolith (Figures 1a, 2a–c and 3(inset image)). The ridges are separated by valleys of varying width. The focus area is discernible as a small pit in the lateral surface (Figure 1a). The medial side of the otolith exhibits a broad and deep sulcus acusticus that is bordered by prominent cristae dorsally and ventrally (Figure 1b). The height map obtained with LSCM of otolith #13 shows that the cristae rise approximately 250 µm above the bottom of the sulcus acusticus (Figure 1b). Anteriorly, the sulcus terminates with a broad opening in the excisura major, while posteriorly, a small notch extends from the sulcus to the excisura minor. Otoliths #4 (Figure 1a) and #13 (Figure 1b) are very close in size (Table 2) despite being one and two years old, respectively, indicating that otolith size is not directly proportional to age across individuals.

Figure 2 shows higher magnification views of the surfaces of otoliths #4 (aged 1 year) and #13 (aged 2 years). The LSCM height map in Figure 2a is a lateral view of the posterior portion of otolith #4. The prominent ridges marked 1–9 converge towards the dorsal and ventral edges of the otolith (top and bottom of the figure, respectively). The broad groove labeled with an asterisk is interpreted as marking the end of the first year of otolith growth. Figure 2b is an SEM-SE image of the posterior portion of otolith #4, covering the labeled region of Figure 2a, but at higher magnification. The white arrow indicates the direction of the most intense otolith growth. Labels 1–9 identify the same ridges as in Figure 2a. In total, 16 prominent ridges could be counted between the focus and the groove labeled by the asterisk, and another six from there up to the otolith's posterior edge.

The yellow arrows in Figure 2b indicate minor incremental markings visible at the otolith surface in the "valleys" between some of the prominent ridges. These minor markings are most clearly seen in the broader valleys between the ridges, i.e., in areas undergoing more rapid growth. Figure 2c is an SEM-SE image of the ventral portion of otolith #13, demonstrating prominent ridges oriented perpendicular or obliquely to the main growth direction and a serrated ventral edge. In places, minor incremental markings (yellow arrows) are also visible in the valleys between the prominent ridges.

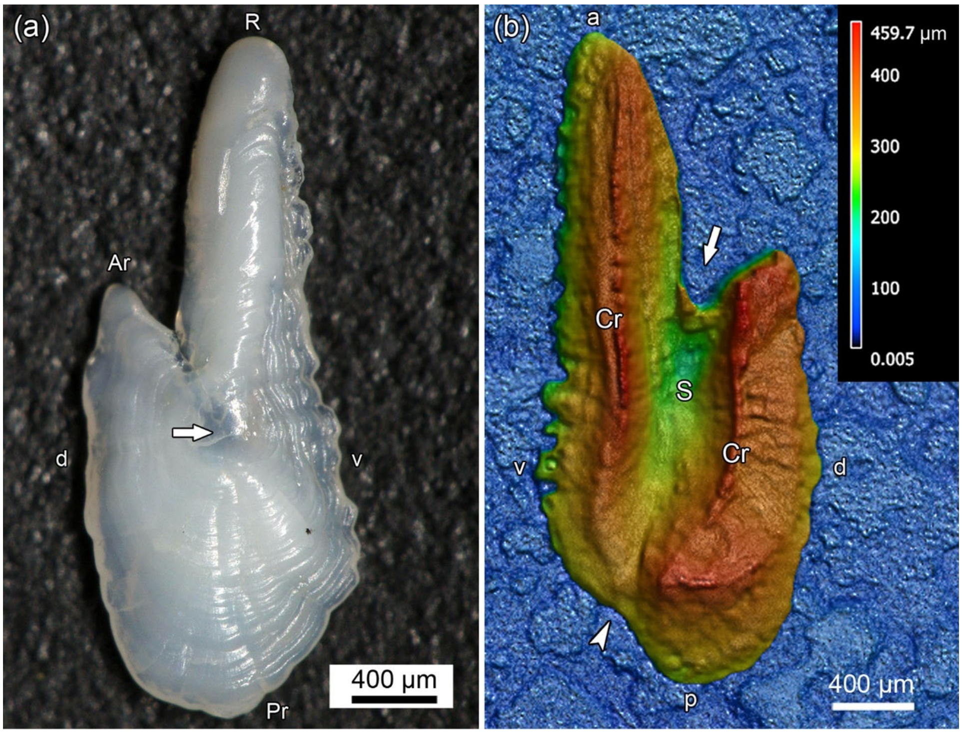

Figure 1. General external morphology of Pacific sardine sagittal otoliths. Letters a, p, v, and d refer to the anterior, posterior, ventral, and dorsal edges of the otoliths, respectively. Anterior is toward the top of the images. (**a**) Reflected light micrograph of otolith #4 (aged 1 year) in lateral view. Ar: Antirostrum, Pr: Postrostrum, R: Rostrum, Arrow: Focus area; (**b**) LSCM micrograph (height map) of otolith #13 (aged 2 years) in medial view. Cr: Crista, S: Sulcus acusticus, Arrow: Excisura major, Arrowhead: Excisura minor.

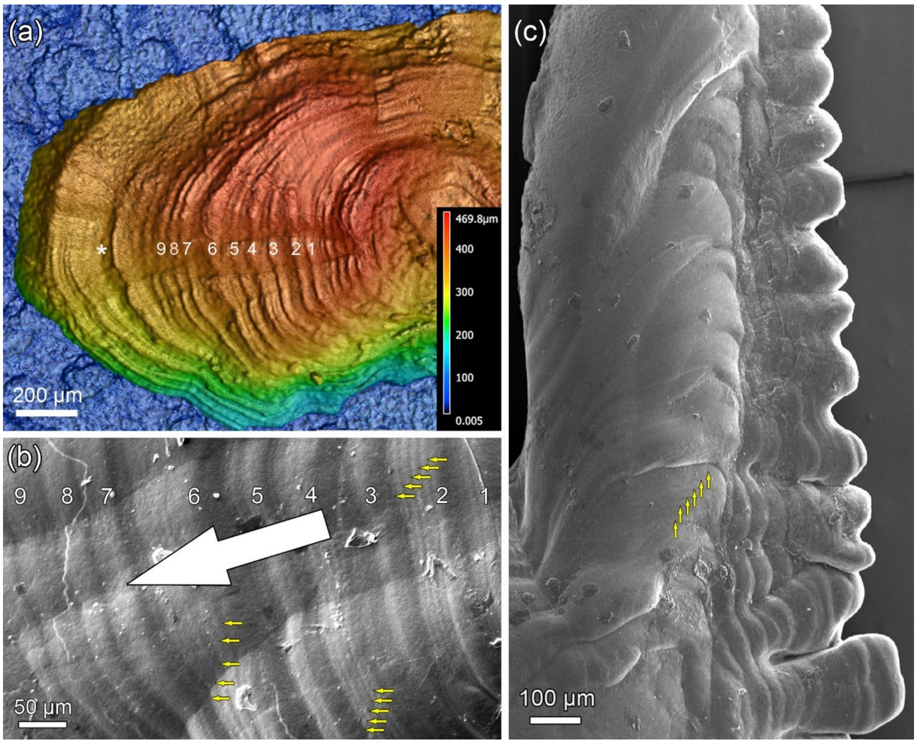

Figure 2. Surface structures of otoliths. (**a**) LSCM micrograph (height map) of the posterior portion of otolith #4 (aged 1 year) in lateral view. Note the prominent ridges that converge towards the dorsal

(top of image) and ventral edges. Numbers 1 to 9 identify the ridges shown at higher magnification in (**b**). Asterisk: prominent groove indicating the end of the first year of otolith growth. (**b**) SEM-SE image of the lateral surface of otolith #4. Nine rounded ridges are marked. Note the presence of minor incremental markings (yellow arrows) in the "valley areas" between some of the prominent ridges. White arrow: Main growth direction of the otolith. (**c**) Ventral portion of otolith #13 (aged 2 years) showing prominent ridges and serrated ventral edge. In places, minor incremental markings (yellow arrows) are discernible between the prominent ridges. Anterior to the top, ventral to the right of the image.

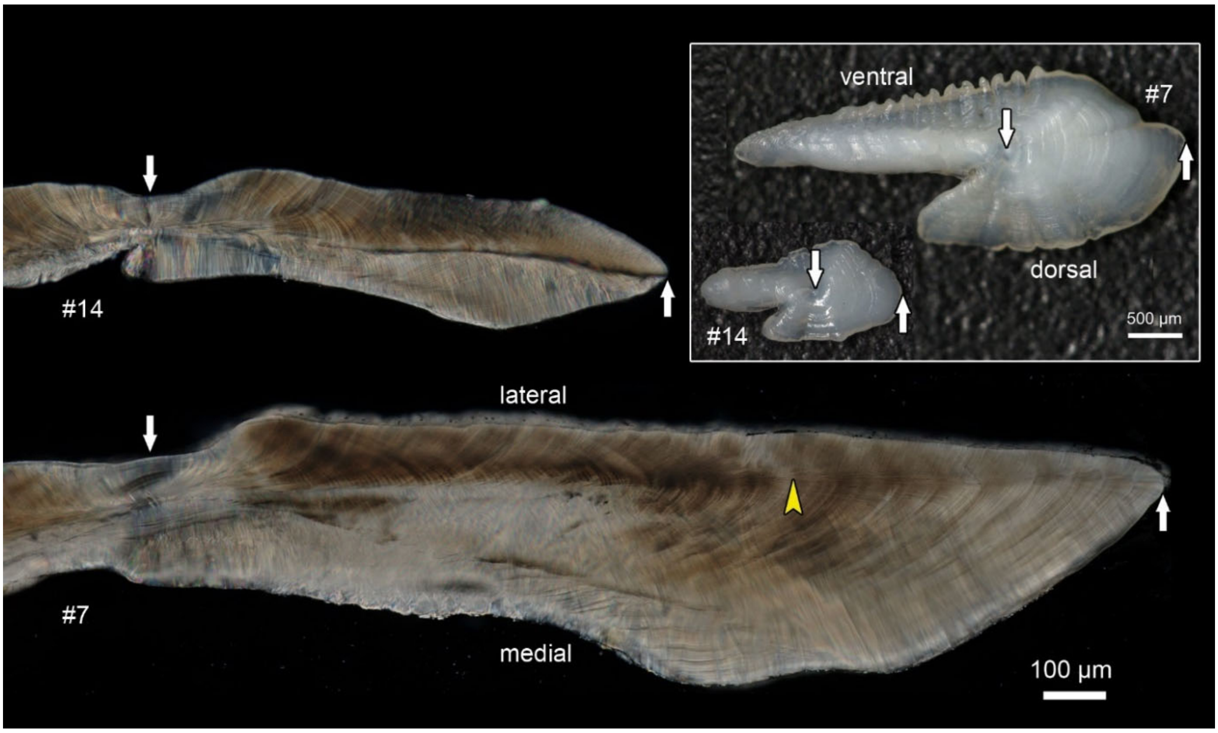

Figure 3. Comparison of the size of sagittal otoliths from an individual less than six months of age (otolith #14) and from an individual aged six years (otolith #7). Shown are micrographs of ground sections viewed under linearly polarized transmitted light. The inset image shows reflected light micrographs of the intact otoliths in lateral view. The downward-directed white arrows mark the focus area and the upward-directed white arrows mark the posterior end of the otoliths. The distance between the two arrows is given as "otolith radius" in Table 2, based on direct measurements of the otoliths. The measurement on the section of otolith #7 produced a slightly higher value. The yellow arrowhead in the ground section of otolith #7 marks the end of the first year of growth. Posterior is to the right of the images. The orientations in #7 also apply to #14.

The width of the otolith's first annual increment is much higher than that of subsequent annual increments (Figure 2a, Figure 3). This is corroborated by measurements on the ground section of otolith #7 from a sardine aged 6 years. While the distance between the focus and the end of the first year's growth, marked by the yellow arrowhead in Figure 3, is 1027 µm, the distance between the focus and the posterior end of the otolith, marked by the upward-directed white arrow, is 1611 µm. Thus, the growth from the end of the first year until death (584 µm) is only 57% of that occurring during the first year of life. In otolith #14, the distance (measured on the ground section) between the focus and the posterior end, reflecting a growth of 152 days (see below), is 838 µm (Figure 3). This indicates a particularly high otolith growth rate during the first months of life. Note that the lengths measured on the ground sections differ slightly (<3%) from those measured on the whole otoliths, as given in Table 2.

3.2. Recording Structures—Daily Increments

Incremental markings diagnosed to reflect a daily (24 h) growth periodicity could readily be identified in the otolith portions formed during the first year of life. With the imaging methods used in the present study, however, daily increments could not reliably be resolved in the otolith portions added during later life. This is attributed to the markedly reduced intensity of accretion following the rapid growth during the first year and the resulting increasingly close spacing of the incremental markings. Each daily increment is a bipartite structure, with the appearance of the two zones depending on the imaging modality used (Figures 4–6, Table 1). In the ground sections viewed under transmitted light or reflected light (with bright background), a daily increment consisted of an inner bright zone, the incremental zone sensu Mugiya et al. [21], and an outer dark (brownish) zone, the discontinuous zone sensu Mugiya et al. [21] (Figures 4 and 5).

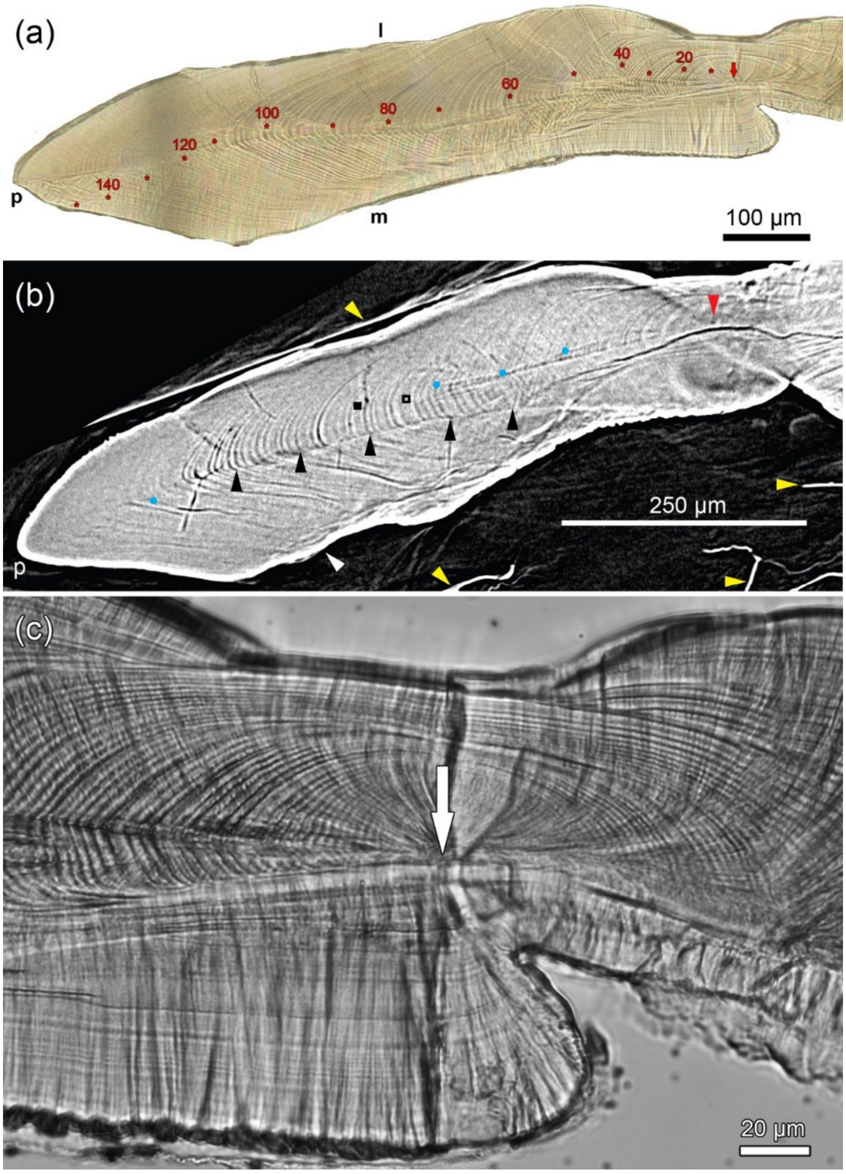

Figure 4. Daily incremental markings in otolith #14. (**a**) Ground section viewed under reflected light (bright background). Between the focus (arrow) and the posterior edge, 152 brownish (dark) markings (discontinuous zones) were counted. Every tenth marking is labeled by an asterisk. Letters l, m, and p refer to the lateral, medial, and posterior edges of the otolith, respectively. (**b**) MicroCT slice (absorption contrast) along roughly the same sectioning plane (no exact match) as the polished

section shown in (**a**). The red arrowhead marks the approximate position of the focus. The black arrowheads mark every tenth dark incremental marking (low-density zone) in an area where they are well visible. The single cyan dot to the left of the black arrowheads marks the distal-most of 10 less visible incremental markings. Between this dot and the posterior end of the otolith (p), there are at least eight faintly visible additional dark incremental markings. The cyan dots on the right side of the image also mark every tenth of a sequence of less visible markings, with two of them corresponding to the two right-most black arrowheads. There are at least 15 faintly visible dark incremental markings between the right-most cyan dot and the focus. The solid black square marks a larger gap between two well-visible light incremental markings, between which two dark markings are barely visible. The unfilled black square marks a similar gap, in which, however, no dark markings can be resolved. In total, we therefore counted 85 dark incremental markings in the slice. White arrowhead: strong X-ray phase contrast at the air–otolith interface, Yellow arrowheads: strong X-ray phase contrast of polymer packing material holding the otolith in place. (**c**) Higher magnification of area around the focus (arrow) as seen in the ground section under plain transmitted light. Note the much better visibility of the incremental markings compared to the microCT image. Also, note that many of the incremental markings do not reach the surface of the otolith and the horizontal orientation of the markings in the lower part of the image (medial portion of the otolith).

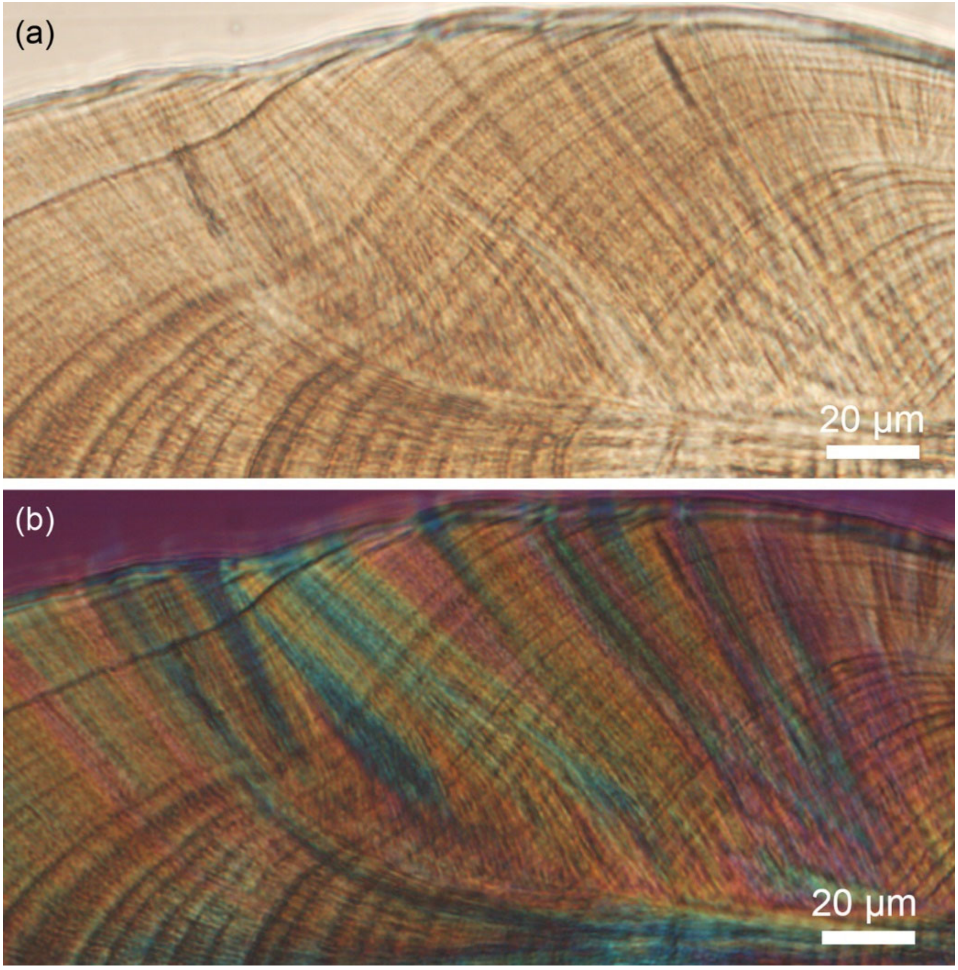

Figure 5. Daily incremental markings in otolith #14 as seen in a ground section viewed under plain train transmitted light (**a**) and under linearly polarized light with a 1λ plate (**b**). In both cases, the discontinuous zones appear dark and the incremental zones bright. Bridging of discontinuous zones by crystallites is visible in places.

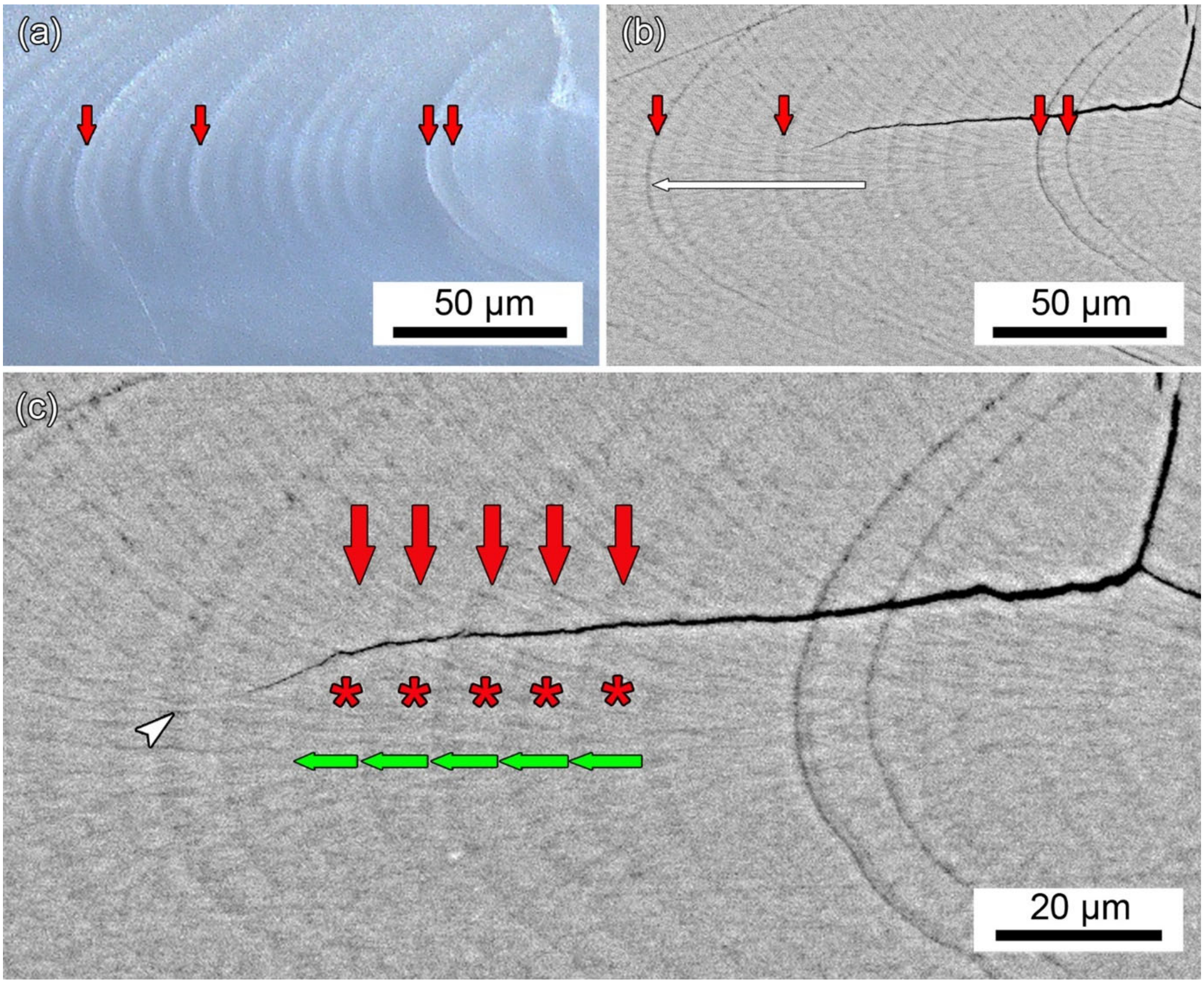

Figure 6. Daily incremental markings in otolith #4 as seen on polished block surface viewed under reflected light (**a**) or by BSE imaging in the SEM (**b**,**c**). Note that the otolith has cracked during processing. (**a**) Under reflected light, the discontinuous zones (four prominent ones are marked by red arrows) appear opaque, while the incremental zones appear translucent. (**b**) In SEM-BSE images, the discontinuous zones appear dark (the four prominent ones marked in (**a**) are indicated by red arrows), while the incremental zones appear bright. White arrow: Main growth direction. (**c**) Higher magnification of the SEM-BSE image. Five consecutive daily increments are marked by green arrows. Each consists of a bright (more mineralized) incremental zone (red asterisks) and a dark (less mineralized) discontinuous zone (red arrows). Arrowhead: Crystallite continuity across a discontinuous zone.

Figure 6 shows images obtained on the polished block surface of otolith #4 (aged 1 year). Under reflected light, the incremental zones appear translucent and the discontinuous zones opaque (Figure 6a), while in SEM-BSE images (Figure 6b,c), the incremental zones appear bright, indicating a higher mineral content, and the discontinuous zones appear dark (lower mineral content). The incremental zones were typically broader than the discontinuous zones, and the width of the daily increments was highest in the direction of main otolith growth (Figures 4–6).

The ground section of otolith #14, viewed under reflected light, showed 152 brownish (dark) incremental markings (=discontinuous zones) between the focus (red arrow) and the posterior edge (Figure 4a). Figure 4b is a microCT slice (absorption contrast) from roughly the same position. The plane of the virtual section is, however, slightly oblique to that of the physical section. A total of 85 dark (low density) incremental markings could be counted in the microCT slice, i.e., this imaging method had a considerably lower ability to resolve the daily increments compared to optical microscopy of ground sections. Figure 4c shows the area around the focus (arrow) in the ground section viewed under plain transmitted light and at higher magnification. Note (1) the much better visibility of the incremental markings compared to the microCT image (Figure 4b), (2) the convergence of the incremental markings that do not reach the lateral surface of the otolith, and (3) the horizontal orientation of the markings in the medial portion of the otolith. As indicated in Table 2, the sardine from which this otolith originated was diagnosed to be substantially younger than one year, and the count of incremental markings in the light micrograph (Figure 4a) is therefore consistent with the daily nature of the increments. The Pacific sardine has a protracted spawning period [49], and a hatch date in March (as suggested by the count) would not be uncommon for the species. Thus, during the first year of life, an exact age-at-death estimation is considered possible based on the counting of daily incremental markings recorded in ground sections of sardine otoliths.

In the plain transmitted light image of Figure 5a, zones of light contrast run from the central portion of the otolith (#14) to its surface (perpendicular to the incremental markings). The continuity of contrast is even more prominent in Figure 5b, an image taken with linearly polarized light and a 1λ plate. In these 2D images, it appears that at least some crystallites bridge the discontinuous zones between adjacent incremental zones, suggesting a certain degree of continuity of the crystalline network across the discontinuous zones. Such crystallite bridging of the discontinuous zones is also supported by SEM-BSE observations. Thus, the white arrowhead in Figure 6c points to a position where light contrast crosses a discontinuous zone, which is consistent with crystalline continuity across this zone.

3.3. Recording Structures—Annual Increments

Figure 7a is a reflected-light image of an intact otolith (#7) submerged in water in a lateral view. In the posterior portion of the otolith, six translucent zones (outer parts of six annual increments, indicating six completed years of growth, are marked with red bars. Figure 7b shows the posterior end of this otolith as seen in a ground section viewed under plain transmitted light, while Figure 7c shows the same region viewed in epifluorescence mode using a GFP filter set. The five boundaries marked by asterisks and numbered 2–6 in Figure 7b,c correspond to the respective outer portions of annual increments 2–6 marked in Figure 7a. The boundaries separate an inner zone, appearing brighter under transmitted light and dark in the epifluorescence image, from an outer zone, which appears brownish under transmitted light and bright in the epifluorescence image. The increased autofluorescence of the latter zone is indicative of a higher organic content.

3.4. Three-Dimensional Examination of Increment Structure

Volumetric microCT allows one to produce 3D renderings of the structure and to numerically section the reconstructed volumes, thereby selecting the most informative orientations. Figure 8a shows a microCT surface rendering of the lateral surface of otolith #7 (with absorption contrast). Ridges and valleys run circumferentially around the otolith, and prominent valleys run radially near the back of the rendering. In the rendering of Figure 8b, the posterior portion of otolith #7 has been removed, exposing a numerical transverse section normal to the otolith's main growth axis.

The alternating light and dark incremental markings are particularly visible on the right-hand side of the section. Figure 8c shows a parasagittal microCT section also reconstructed with absorption contrast; dark zones contain less mineral than light zones in this panel as well as in Figure 8d,e. Incremental markings are particularly clear near the focus (the lowest portion of the image), and additional markings can be seen within the volume leading to the otolith's posterior end. Figure 8d shows a parasagittal section of otolith #7 (as does Figure 8c) but reconstructed with the Paganin algorithm ([46], X-ray phase contrast). The increment structure is clearer with X-ray phase contrast (Figure 8d) than with absorption contrast (Figure 8c). The boxed area of Figure 8d is enlarged in Figure 8e, showing every other slice in a 40 μm thick volume. Red disks mark two prominent dark (weaker contrast) zones in each slice of Figure 8e, and in slice 1, two weaker contrast zones are clearly visible between the prominent increments. The other slices show that these zones have quite variable contrast even a few micrometers from slice 1, and in some slices, the contrast is so weak that zones would be missed (e.g., slice 19). Slice images (absorption contrast) appear in Supplementary Figure S1, and Table 3 provides information on the number of dark zones and the width of the light and dark zones as recorded with absorption contrast from microCT.

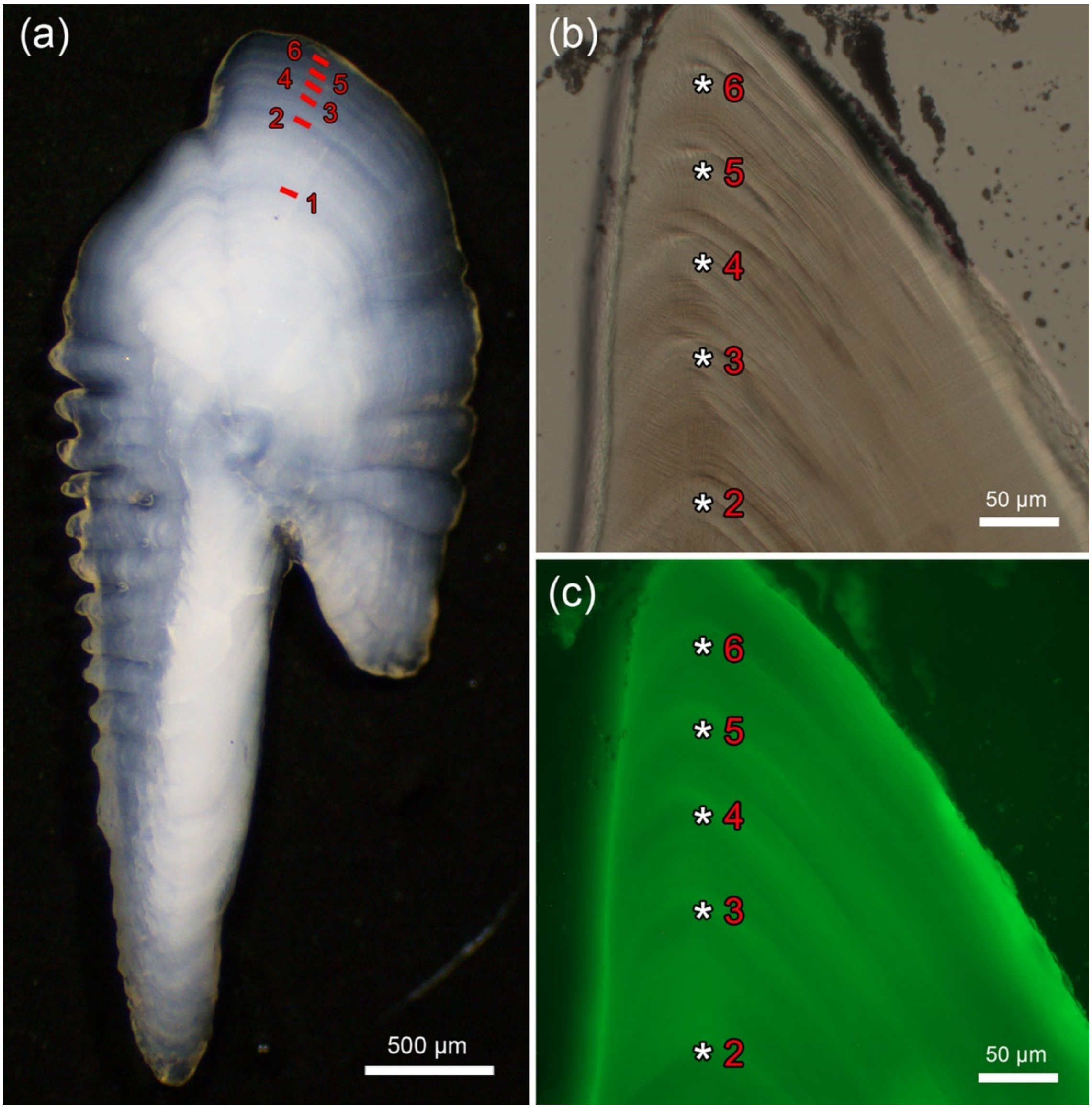

Figure 7. Annual growth marks in otolith #7 (aged 6 years). (**a**) Reflected light image of the otolith submerged in water in lateral view. Six translucent increments (outer parts of six annuli) are marked in the posterior portion. (**b**,**c**) Micrographs of ground section viewed under plain transmitted light (**b**) and in epifluorescence mode using a GFP filter set (**c**). Shown is the otolith's posterior portion with five boundaries (marked by asterisks and numbered 2–6) that correspond to the respective outer portions of the annual increments 2–6 marked in (**a**). The boundaries separate an inner zone, appearing brighter under transmitted light and dark in the epifluorescence image, from an outer zone, which appears brownish under transmitted light and bright in the epifluorescence image. The increased autofluorescence of the latter zone is indicative of a higher organic content. Posterior to the top, ventral to the left of the images.

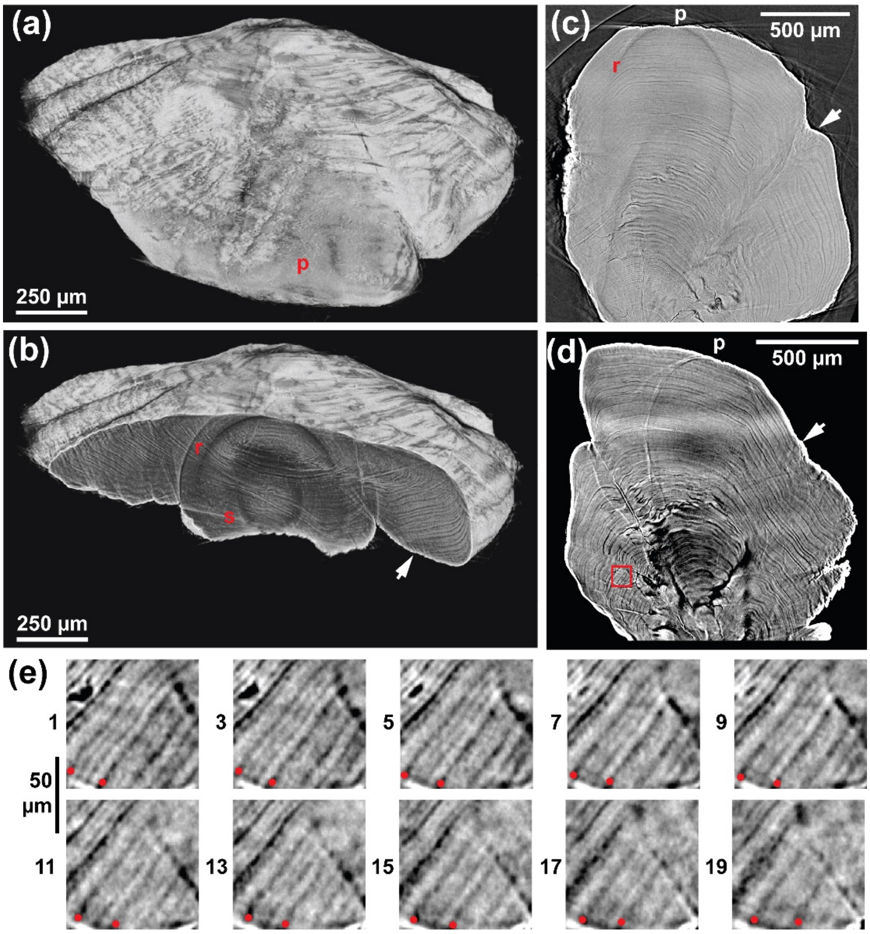

Figure 8. MicroCT images of otolith #7. (**a**) 3D surface rendering of the otolith with the posterior end (p) toward the viewer, the dorsal edge is to the left, and the lateral surface is shown. Absorption contrast. (**b**) Virtual section through the rendering (the same orientation as in panel (**a**), also absorption contrast) reveals the increments within the otolith. The medial surface is at the bottom of the section. The white border at the surface of the otolith (white arrow) is X-ray phase contrast at the air–solid interface. There are reconstruction artifacts on either side of "r" (ring artifacts) and at "s" (a streak artifact). (**c**) Parasagittal section of the otolith with absorption contrast. p: posterior end, r: ring artifact, white arrow: X-ray phase contrast at the air–solid interface. (**d**) Parasagittal slice reconstructed with X-ray phase contrast (Paganin filter) in a slightly different orientation than in (**c**). The red box indicates the area enlarged in panel (**e**). p: posterior end, white arrow: X-ray phase contrast at the air–solid interface. (**e**) Stack of 20 slices (covering 40 μm thickness) along the direction perpendicular to the plane shown in panel (**d**); every other slice is shown and labeled with the numeral to the left of the image. In each image, the matching pair of prominent dark increments (low phase contrast) is labeled with red disks.

Table 3. Counts and measurements of microCT images from five otoliths. Distance is from first counted zone to last counted zone; this distance is less than the otolith radius as zones were not identified throughout the length of the radius. High-density areas with low resolution (unable to resolve low-density zones) were excluded from the calculation of the high-density average.

Otolith	Number of Low Density Zones	Distance (μm)	Average Low Density Zone Periodicity (μm/low Density Zone)	Average Width (Range) of Low Density Zones (μm)	Average Width (Range) of High Density Zones (μm)
#4	44	405.79	9.23	3.22 (1.55–5.39)	5.25 (2.07–8.42)
#7	138	1440.96	10.44	2.26 (1.38–4.63)	5.46 (1.38–11.11)

Table 3. *Cont.*

Otolith	Number of Low Density Zones	Distance (µm)	Average Low Density Zone Periodicity (µm/low Density Zone)	Average Width (Range) of Low Density Zones (µm)	Average Width (Range) of High Density Zones (µm)
#13	75	668.53	8.91	2.98 (2.07–4.63)	5.35 (2.49–15.46)
#14	49	370.55	7.56	2.47 (2.07–3.52)	5.11 (2.07–8.42)
#83	82	725.94	8.85	2.17 (1.55–3.52)	3.68 (1.55–9.87)

3.5. Fluorochrome-Labeled Otolith

Figure 9 shows the posterior end of otolith #83, which was labeled with OTC one year before the sardine's death. The micrograph of Figure 9a is an overlay image of the transmitted light channel and the fluorescence channel. The arrow indicates the OTC label. Note the convergence of the incremental markings in the posterior direction in the area encircled by the white oval, indicating variation in the growth rate along the circumference of the otolith, even along a nearly identical anatomical direction. Figure 9b is a transmitted-light image taken at a higher magnification. An accentuated incremental marking is co-localized with the OTC label (green crosses), suggesting that the OTC injection had caused a disturbance/disruption ("check") in the otolith's growth process. The red asterisks identify 40 incremental markings that could be identified between the accentuated marking/OTC label and the otolith surface. As this distance represents growth over one year, the markings are clearly not of a daily nature, and daily increments could therefore not be resolved in the otolith portion formed during the year of captive growth.

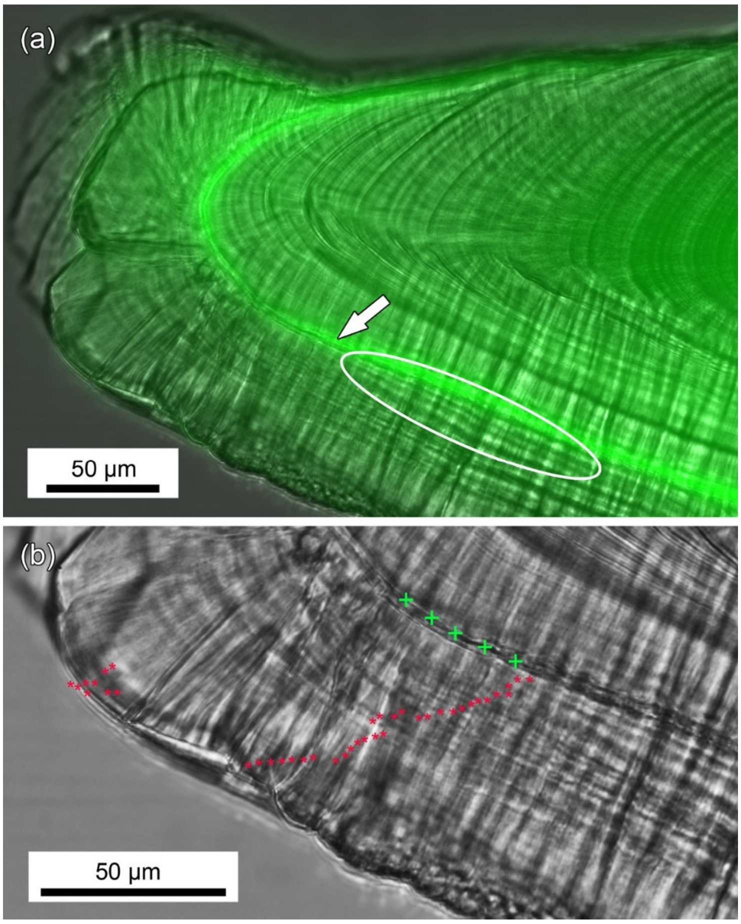

Figure 9. Light micrographs of ground section of otolith #83, labeled with oxytetracycline (OTC) one year before death. (**a**) Overlay image of transmitted light and fluorescence channels. Arrow: OTC

label. Note the convergence of incremental markings in posterior direction in the area marked by the white oval. (**b**) Higher magnification of plain transmitted light image of the ground section, demonstrating co-localization of OTC label (position marked by green crosses) and an accentuated incremental marking. Red asterisks indicate incremental markings ($n = 40$) identified between the OTC label and the otolith surface.

4. Discussion

The present study used a variety of imaging modalities to analyze the incremental markings present in the sagittal otolith of the Pacific sardine. Some approaches (LSCM and synchrotron microCT) were applied to otoliths for the first time. The use of multiple imaging modalities allows the comparison of the advantages and limitations of the various methods and a cross-validation of their results.

The marked system of prominent ridges and valleys characterizing the surface of the otoliths has thus far not received much attention. It is currently unclear whether the structures visible at the otolith surface, i.e., the prominent ridges and valleys as well as the minor markings in the valley regions, represent periodic growth signals that could be used for age estimation. Both fortnight (14 days) and lunar (28 days) increments have been identified in other fish species [20,24,50]. The periodicity of these ridges may reflect a lunar cycle as otolith #14 had 16 ridges in the first year of growth. Further studies addressing this question are therefore encouraged, as these structures can be readily visualized and measured by LSCM. This method thus allows for the rapid automated surface profiling of otoliths and might therefore be a useful addendum to the toolkit of fish biologists working on age estimation.

Our results confirm that incremental markings reflecting different growth periodicities are present in the otoliths and that the intensity of the growth process is highly variable both temporally and spatially [22,23]. Thus, the velocity of otolith growth slows down dramatically after the first year and the accretion of new material varies considerably along the otolith’s circumference. This leads to the convergence of incremental markings in certain areas. There are apparently also surfaces where almost no growth occurs over a certain period of time, while simultaneously, the accretion of new material continues in other regions of the otolith. Corresponding observations have been made in the case of bone growth [7,51]. Finally, the microCT results on successive slices (Figure 8e) show that incremental markings can be clearly visible in one volume but are invisible a few tens of micrometers away. The orientation dependence of increment spacing and their variable contrast present real challenges in analyzing increment periodicities.

Daily increments in the otoliths of the Pacific sardine can be readily visualized by optical microscopy and BSE imaging in the SEM, and the appearance of the incremental and discontinuous zones corresponds to what is known from the literature for other fish species [9,22]. The daily increments are most visible and thus countable along the main growth direction of the otolith, where their width is the largest. It was, however, not possible to reliably resolve daily increments beyond the first year of otolith growth with the imaging methods used in the present study. This is attributed to the narrowing of the incremental markings with reduced growth intensity, and the resulting reduced width and spacing of the markings being beyond the resolving power of our methods.

The ability of microCT, at least at the resolution level used in the present study, to resolve the finest-scale incremental markings is lower than that of the optical and SEM-BSE methods used in the present study. Generally, phase contrast imaging is better suited for the visualization of daily increments by microCT than absorption contrast imaging. Improving the resolution in microCT will likely increase the applicability of the method. For example, ID19, the European Synchrotron Radiation Facility, can routinely provide full field microCT with voxels as small as 150 nm [52], and the lens-based nanoCT instrument at 32-ID, APS, routinely provides imaging with 50 nm voxels on 50 μm diameter specimens [53]. Laboratory nanoCT systems producing reconstructions with sub-micrometer voxels are available from several manufacturers. The voxel size used in the present study (0.69 μm) was already suited to provide general information on otolith microstructures using a non-destructive approach. Another method with the potential to resolve thin, closely spaced incremental markings could be SEM-SE imaging of etched polished surfaces at high (>10,000×) magnification.

Recently, Hay et al. [40] reported that daily increments in pipefish otoliths, in which the increment count is also hampered by lack of resolution of standard microscopic methods, can be resolved based on a periodic alternation of zones with low and high sulfur (S) content as revealed by synchrotron-based scanning X-ray fluorescence. They found that the (mineral-rich) light zones (L-zones), corresponding to the incremental zones of Mugiya et al. [21], had a low S content, while dark zones (D-zones, rich in organic matter), corresponding to the discontinuous zones of Mugiya et al. [21], showed higher S concentrations. Hay et al. [40] suggest that the high S content in the D-zones is caused by the increased incorporation of S-rich proteoglycans during growth compared to the L-zones. It seems worthwhile to also explore the potential ability of X-ray fluorescence analysis to resolve daily incremental markings throughout entire otoliths in the Pacific sardine from individuals older than one year.

Our results suggest some continuity of the crystalline network between consecutive incremental zones, i.e., that there is crystallite bridging across the intervening discontinuous zone. This confirms previous statements by other authors and their conclusion that the term discontinuous zone is therefore somewhat misleading [22]. Although it was not noted explicitly in the Results, microCT also showed light contrast bands extending radially through discontinuous zones; these radial bands have variable thicknesses both in the plane of the reconstructed slices and perpendicular to this plane.

Annual increments could be demonstrated using the established method of counting them in submerged otoliths. The analysis of ground sections suggests that the zones appearing bright in transmitted light micrographs of polished sections and dark under epifluorescence are more mineralized and contain less organic material than the zones appearing dark in the transmitted light micrographs and bright under epifluorescence. Using ground sections to count annual increments is a viable method; however, it is more labor-intensive to produce ground sections than the current method of counting annual increments from submerged whole otoliths.

As the daily apposition of new growth layers of otoliths continues over the entire life of a fish, although at highly varying rates, the relationship between daily increments and annual increments needs to be resolved. This question does not appear to have attracted much interest in the past. It may be assumed that within an annual increment, the volume ratio of the (daily) discontinuous to incremental zones is higher in the annual opaque zones rich in organic material (showing higher autofluorescence) than in the more mineralized annual translucent zones. Alternatively, it could be that both the incremental and the discontinuous zones within the high organic annual opaque zones are less mineralized and contain more organicmatrix than those within the low organic annual translucent zones.

In vivo fluorochrome labeling is an established method used to reconstruct the growth of mineralized tissues [54–56]. OTC injection in the Pacific sardine otolith produced a distinct, well-visible label in the otolith. By labeling at multiple time points during otolith growth, using either the same or different fluorochromes, it is possible to precisely reconstruct the velocity of otolith growth as well as the variation in the accretion rate along the otolith surface. Experiments using repeated labeling of growing otoliths are therefore encouraged. In the present study, the OTC dose caused the formation of an accentuated incremental line in the otolith, indicating a certain disruption of the growth process. Similar observations have previously been made with OTC labeling of forming enamel [57]. Such growth disruption could likely be prevented by using a lower dosage of OTC or a different fluorochrome, e.g., calcein.

5. Conclusions

The four imaging modalities used to study incremental markings in sagittal otoliths of the Pacific sardine (*Sardinops sagax*), namely SEM-BSE, light microscopy, LSCM, and synchrotron microCT, all revealed that the intensity of the growth process is highly variable both temporally and spatially. This first use of LSCM on fish otoliths demonstrated that the ridges and valleys of the external surface could be efficiently quantified in 3D; the ridges and valleys observed here may correspond to fortnight or lunar (28 days) increments, similar to those documented in other fish species. Compared to SEM and microCT instruments, LSCM is relatively inexpensive and might prove to be a tool useful to fish biologists working on age estimation. Daily increments could not be identified beyond the first year, but in the first year, they were clear in SEM-BSE and optical micrographs of polished sections. Synchrotron microCT could also demonstrate increments within the volume grown during the first year, but there was a smaller number visible than observed with SEM-BSE and optical microscopy. It may be that SEM-BSE and/or synchrotron microCT imaging with higher resolutions (than was used in this study) may be able to reveal daily increments beyond the first year.

Supplementary Materials: The following supporting information can be downloaded at: https://www.mdpi.com/article/10.3390/min14070705/s1, Figure S1: Composite microCT images of re-sliced sections of 5 otoliths: otolith #4, #7, #13, #14, and #83. Red dots, when present, denote the focus. Cyan marks each low density zone. Black line indicates distance measured for incremental marking frequency (Table 3). Right is posterior, top is lateral, and bottom is medial.

Author Contributions: Conceptualization, K.C.J., U.K., S.R.S. and H.K.; methodology, K.C.J., U.K., S.R.S. and H.K.; formal analysis, K.C.J., U.K., S.R.S. and H.K.; investigation, K.C.J., U.K., V.C., S.R.S. and H.K.; resources, all authors.; writing—original draft preparation, K.C.J., U.K., S.R.S. and H.K.; writing—review and editing, all authors; visualization, V.C. and V.N. All authors have read and agreed to the published version of the manuscript.

Funding: This research received no external funding.

Data Availability Statement: The data are available under reasonable request.

Acknowledgments: This research used resources of the Advanced Photon Source, a U.S. Department of Energy (DOE) Office of Science User Facility, operated for the DOE Office of Science by Argonne National Laboratory under Contract No. DE-AC02-06CH11357. Argonne National Laboratory's work was supported by the U.S. Department of Energy, Office of Science, Office of Basic Energy Sciences, under contract DE-AC02-06CH11357.

Conflicts of Interest: Aside from the aforementioned contracts, this research did not receive any specific grants from funding agencies in the public, commercial, or nonprofit sectors. Further, these funding agencies had no role in any aspect of this study. The authors note they have no conflicts of interest.

References

1. Klevezal, G.A. *Recording Structures of Mammals*; Balkema: Rotterdam, The Netherlands, 1996.
2. Nanci, A. (Ed.) *Ten Cate's Oral Histology: Development, Structure, and Function*, 9th ed.; Elsevier: Amsterdam, The Netherlands, 2017.
3. Naji, S.; Rendu, W.; Gourichon, L. (Eds.) *Cementum in Anthropology*; Cambridge University Press: Cambridge, UK, 2022.
4. Peharda, M.; Schöne, B.R.; Black, B.A.; Corrège, T. Advances in sclerochronology research in the last decade. *Palaeogeo. Palaeoclim. Palaeoecol.* **2021**, *570*, 110371. [CrossRef]
5. Stringer, C.A.; Prendergast, A.L. Freshwater mollusc sclerochronology: Trends, challenges and future directions. *Earth-Sci. Rev.* **2023**, *247*, 104621. [CrossRef]
6. Natanson, L.J.; Skomal, G.B.; Hoffmann, S.L.; Porter, M.F.; Goldman, K.J.; Serra, D. Age and growth of sharks: Do vertebral band pairs record age? *Mar. Freshw. Res.* **2018**, *69*, 1440–1452. [CrossRef]
7. Francillon-Vieillot, H.; Buffrénil V de Castanet, J.; Géraudie, J.; Meunier, F.J.; Sire, J.Y.; Zylberberg, L.; de Ricqlès, A. Microstructure and mineralization of vertebrate skeletal tissues. In *Skeletal Biomineralization: Patterns, Processes and Evolutionary Trends*; Carter, J.G., Ed.; Van Nostrand Reinhold: New York, NY, USA, 1990; Volume 1, pp. 471–530.
8. Oschmann, W. Sclerochronology: Editorial. *Int. J. Earth Sci.* **2009**, *98*, 1–2. [CrossRef]

9. Campana, S.E. Chemistry and composition of fish otoliths: Pathways, mechanisms and applications. *Mar. Ecol. Prog. Ser.* **1999**, *188*, 263–297. [CrossRef]
10. Campana, S.E. Otolith science entering the 21st century. *Mar. Freshw. Res.* **2005**, *56*, 485–495. [CrossRef]
11. James, K.C.; Dorval, E.; Erisman, B.E. Validation of periodicity of growth band formation in Pacific sardine (*Sardinops sagax*) from a captive growth experiment. *Mar. Biol.* **2024**, *171*, 105. [CrossRef]
12. Schulz-Mirbach, T.; Ladich, F.; Plath, M.; Heß, M. Enigmatic ear stones: What we know about the functional role and evolution of fish otoliths. *Biol. Rev.* **2019**, *94*, 457–482. [CrossRef] [PubMed]
13. Retzius, G. *Das Gehörorgan der Wirbelthiere. I. Das Gehörorgan der Fische und Amphibien*; Samson & Wallin: Stockholm, Sweden, 1881; pp. 1–222, 35 plates.
14. Wohlfahrt, T.A. Das Ohrlabyrinth der Sardine (*Clupea pilchardus* Walb.) und seine Beziehungen zur Schwimmblase und Seitenlinie. *Z. Morphol. Ökol. Tiere* **1936**, *31*, 371–410. [CrossRef]
15. Degens, E.T.; Deuser, W.F.G.; Haedrich, R.L. Molecular structure and composition of fish otoliths. *Mar. Biol.* **1969**, *2*, 105–113. [CrossRef]
16. Borelli, G.; Mayer-Gostan, N.; Merle, P.L.; De Pontual, H.; Boeuf, G.; Allemand, D.; Payan, P. Composition of biomineral organic matrices with special emphasis on turbot (*Psetta maxima*) otolith and endolymph. *Calcif. Tiss. Int.* **2003**, *72*, 717–725. [CrossRef] [PubMed]
17. Lundberg, Y.W.; Xu, Y.; Thiessen, K.D.; Kramer, K.K. Mechanisms of otoconia and otolith development. *Dev. Dyn.* **2015**, *244*, 239–253. [CrossRef]
18. Dunkelberger, D.A.; Dean, J.M.; Watabe, N. The ultrastructure of the otolithic membrane and otolith in the juvenile mummichog, *Fundulus heteroclitus*. *J. Morphol.* **1980**, *163*, 367–377. [CrossRef] [PubMed]
19. Popper, A.N.; Hoxter, B. The fine structure of the sacculus and lagena of teleost fish. *Hear. Res.* **1981**, *5*, 245–263. [CrossRef] [PubMed]
20. Panella, G. Fish otoliths: Daily growth layers and periodical patterns. *Science* **1971**, *173*, 1124–1127. [CrossRef] [PubMed]
21. Mugiya, Y.; Watabe, N.; Yamada, J.; Dean, J.M.; Dunkelberger, D.G.; Shimizu, M. Diurnal rhythm in otolith formation in the goldfish, *Carassius auratus*. *Comp. Biochem. Physiol.* **1981**, *68A*, 659–662. [CrossRef]
22. Campana, S.E.; Neilson, J.D. Microstructure of fish otoliths. *Can. J. Fish. Aquatic. Sci.* **1985**, *42*, 1014–1032. [CrossRef]
23. Campana, S.E. Measurement and interpretation of the microstructure of fish otoliths. In *Otolith Microstructure Examination and Analysis*; Stevenson, D.K., Campana, S.E., Eds.; Canadian Special Publication of Fisheries and Aquatic Sciences; Fisheries and Oceans Canada: Ottawa-Ontario, BC, Canada, 1992; Volume 117, pp. 59–71.
24. Campana, S.E. Lunar cycles of otolith growth in the juvenile starry flounder *Platichthys stellatus*. *Mar. Biol.* **1984**, *80*, 239–246. [CrossRef]
25. Gauldie, R.W. Function, form and time-keeping properties of fish otoliths. *Comp. Biochem. Physiol.* **1988**, *91A*, 395–402. [CrossRef]
26. Morales-Nin, B. Review of the growth regulation processes of otolith daily increment formation. *Fish. Res.* **2000**, *46*, 53–67. [CrossRef]
27. Mugiya, Y. Phase difference between calcification and organic matrix formation in the diurnal growth of otoliths in the rainbow trout, *Salmo gairdneri*. *Fish. Bull.* **1987**, *85*, 395–401.
28. Gauldie, R.W.; Nelson, D.G.A. Aragonite twinning and neuroprotein secretion are the cause of daily growth rings in fish otoliths. *Comp. Biochem. Physiol.* **1988**, *97A*, 461–474. [CrossRef]
29. Reis-Santos, R.; Gillanders, B.M.; Sturrock, A.M.; Izzo, C.; Oxman, D.S.; Lueders-Dumont, J.A.; Hüssy, K.; Tanner, S.E.; Rogers, T.; Doubleday, Z.A.; et al. Reading the biomineralized book of life: Expanding otolith biogeochemical research and applications for fisheries and ecosystem-based management. *Rev. Fish Biol. Fish.* **2023**, *33*, 411–449. [CrossRef]
30. Buckmeier, D.L.; Sakaris, P.C.; Schill, D.J. Validation of annual and daily increment in calcified structures and verification of age estimates. In *Age and Growth of Fishes: Principles and Techniques*; Quist, M.C., Isermann, D.A., Eds.; American Fisheries Society: Bethesda, MD, USA, 2017; pp. 33–79.
31. Jones, C.M. Age and growth. In *Fishery Science: The Unique Contribution of Early Life Stages*; Fuiman, L.A., Werner, R.G., Eds.; Blackwell Scientific Publications: Oxford, UK, 2002; pp. 33–63.
32. Secor, D.H.; Dean, J.M.; Laban, E.H. *Manual for Otolith Removal and Preparation for Microstructural Examination*; Technical Report 91-1; University of South Carolina, Branch Institute for Marine Biology and Coastal Research: Columbia, SC, USA, 1991.
33. Beckman, D.W.; Wilson, C.A. Seasonal timing of opaque zone formation in fish otoliths. In *Recent Developments in Fish Otolith Research*; Secor, D.H., Dean, J.M., Campana, S.E., Eds.; University of South Carolina Press: Columbia, SC, USA, 1995; pp. 27–43.
34. Hüssy, K.; Krüger-Johnsen, M.; Thomsen, T.B.; Heredia, B.D.; Næraa, T.; Limburg, K.E.; Heimbrand, Y.; McQueen, K.; Haase, S.; Krumme, U.; et al. It's elemental, my dear Watson: Validating seasonal patterns in otolith chemical chronologies. *Can. J. Fish. Aquatic. Sci.* **2021**, *78*, 551–556. [CrossRef]
35. Beamish, R.J.; McFarlane, G.A. The forgotten requirement for age validation in fisheries biology. *Trans. Am. Fish. Soc.* **1983**, *112*, 735–743. [CrossRef]
36. Dorval, E.; McDaniel, J.D.; Macewicz, B.J.; Porzio, D.L. Changes in growth and maturation parameters of Pacific sardine *Sardinops sagax* collected off California during a period of stock recovery from 1994 to 2010. *J. Fish. Biol.* **2015**, *87*, 286–310. [CrossRef] [PubMed]

37. Kuriyama, P.T.; Zwolinski, J.P.; Hill, K.T.; Crone, P.R. *Assessment of the Pacific sardine resource in 2020 for U.S. Management in 2020–2021*; NOAA Technical Memorandum NMFS-SWFSC-628; National Oceanic and Atmospheric Administration: Washington, DC, USA, 2020.
38. Butler, J.L. Comparisons of the Larval and Juvenile Growth and Larval Mortality of Pacific Sardine and Northern Anchovy and Implications for Species Interaction. PhD Thesis, University of California San Diego, San Diego, CA, USA, 1987.
39. Barnes, J.T.; Foreman, T.J. Recent evidence for the formation of annual growth increments in the otoliths of young Pacific sardines (*Sardinops sagax*). *Calif. Dept. Fish Game* **1994**, *80*, 29–30.
40. Hay, V.; Berland, S.; Medjoubi, K.; Somogyi, A.; Mennesson, M.I.; Keith, P.; Lord, C. Unmasking pipefish otolith using synchrotron-based scanning X-ray fluorescence. *Sci. Rep.* **2023**, *13*, 4794. [CrossRef] [PubMed]
41. Yaremko, M.L. *Age Determination in Pacific Sardine, Sardinops sagax*; NOAA Technical Memorandum NMFS-SWFSC-223; National Oceanic and Atmospheric Administration: Washington, DC, USA, 1996.
42. Fitch, J.E. Age composition of the southern California catch of Pacific mackerel 1939–40 through 1950–51. *Calif. Dept. Fish Game* **1951**, *83*, 1–73.
43. Boyde, A.; Jones, S.J. Backscattered electron imaging of dental tissues. *Anat. Embryol.* **1983**, *168*, 211–226. [CrossRef] [PubMed]
44. Skedros, J.G.; Bloebaum, R.D.; Bachus, K.N.; Boyce, T.M. The meaning of graylevels in backscattered electron images of bone. *J. Biomed. Mater. Res.* **1993**, *27*, 47–56. [CrossRef] [PubMed]
45. Nikitin, V.; Tekawade, A.; Duchkov, A.; Shevchenko, P.; De Carlo, F. Real-time streaming tomographic reconstruction with on-demand data capturing and 3D zooming to regions of interest. *J. Synchrotron. Rad.* **2022**, *29*, 816–828. [CrossRef] [PubMed]
46. Paganin, D.; Mayo, S.C.; Gureyev, T.E.; Miller, P.R.; Wilkins, S.W. Simultaneous phase and amplitude extraction from a single defocused image of a homogeneous object. *J. Microsc.* **2002**, *206*, 33–40. [CrossRef] [PubMed]
47. Nikitin, V. TomocuPy—Efficient GPU-based tomographic reconstruction with asynchronous data processing. *J. Synch. Rad.* **2023**, *30*, 179–191. [CrossRef] [PubMed]
48. Schindelin, J.; Arganda-Carreras, I.; Frise, E.; Kaynig, V.; Longair, M.; Pietzsch, T.; Preibisch, S.; Rueden, C.; Saalfeld, S.; Schmid, B.; et al. Fiji: An open-source platform for biological-image analysis. *Nat. Meth.* **2012**, *9*, 676–682. [CrossRef] [PubMed]
49. Ahlstrom, E.H. Distribution and abundance of eggs of the Pacific Sardine, 1952–1956. *Fish. Bull.* **1959**, *60*, 185–213.
50. Panella, G. Otolith growth patterns: An aid in age determination in temperate and tropical fishes. In *Ageing of Fish*; Bagenal, T.B., Ed.; Unwin Brothers Limited: London, UK, 1974; pp. 28–39.
51. De Buffrénil, V.; Quilhac, A. Basic processes in bone growth. In *Vertebrate Skeletal Histology and Paleohistology*; de Buffrénil, V., de Ricqles, A.J., Zylberberg, L., Padian, K., Eds.; CRC Press: Boca Raton, FL, USA, 2021; pp. 193–220.
52. Rack, A.; (ESRF, Grenoble, France). Personal communication, 2024.
53. Nikitin, V.; (APS, Argonne National Laboratory, Lemon, IL, USA). Personal communication, 2024.
54. Bromage, T.G. Enamel incremental periodicity in the pig-tailed macaque: A polychrome fluorescent labeling study of dental hard tissues. *Am. J. Phys. Anthropol.* **1991**, *86*, 205–214. [CrossRef]
55. Van Gaalen, S.M.; Kruyt, M.C.; Geuze, R.E.; de Bruijin, J.D.; Alblas, J.; Dhert, W.J.A. Use of fluorochrome labels in in vivo bone tissue engineering research. *Tiss. Eng. Part B Rev.* **2010**, *16*, 209–217. [CrossRef] [PubMed]
56. Emken, S.; Witzel, C.; Kierdorf, U.; Frölich, K.; Kierdorf, H. Characterization of short-period and long-period incremental markings in porcine enamel and dentine–Results of a fluorochrome labelling study in wild boar and domestic pigs. *J. Anat.* **2021**, *239*, 1207–1220. [CrossRef] [PubMed]
57. Kierdorf, H.; Kierdorf, U.; Frölich, K.; Witzel, C. Lines of evidence–Incremental markings in molar enamel of Soay sheep as revealed by a fluorochrome labeling and backscattered electron imaging study. *PLoS ONE* **2013**, *8*, e74597. [CrossRef]